JOURNAL OF COMPUTATIONAL PHYSICS **139,** 166–183 (1998)
ARTICLE NO. CP975868

Evaluation of the Perfectly Matched Layer for Computational Acoustics

Quan Qi and Thomas L. Geers

Center for Acoustics, Mechanics and Materials, Department of Mechanical Engineering, University of Colorado, Boulder, Colorado
E-mail: geers@spot.colorado.edu

Received July 19, 1996; revised September 11, 1997

The perfectly matched layer (PML) recently formulated by Berenger for the absorption of radiated/scattered waves in computational electromagnetics is adapted to computational acoustics, and its effectiveness as a nonreflecting boundary is examined. The excellent absorbing ability of the PML is demonstrated by its small reflection coefficient for a plane wave incident on a plane interface. However, additional frequency-domain and time-domain solutions show that the PML may not be an appropriate computational boundary if the analyst is only interested in the response of the radiator/scatterer and/or the acoustic field in the vicinity of the radiator/scatterer. © 1998 Academic Press

1. INTRODUCTION

In 1994, Berenger [1] presented, for the finite-difference, time-domain solution of Maxwell's equations in two dimensions, a new absorbing boundary, which he called a perfectly matched layer (PML). His demonstration that the PML possesses extraordinary energy-absorbing properties was verified by Katz *et al*. [2], who also extended the formulation to three dimensions. Recently, Hu [3] formulated a PML for the linearized Euler equations in two dimensions; similar energy-absorbing effectiveness was demonstrated.

A PML is described by governing equations produced through the introduction of artificial attenuation into the governing equations for the enclosed medium. Thus, the domain of the PML may be discretized in the same manner as that employed to discretize the enclosed medium.

Here, the PML is examined for computational acoustics. First, the full 3D acoustic formulation is constructed. Next, the reflection of plane waves at the unbounded flat interface between a semi-infinite acoustic domain and a semi-infinite acoustic PML is investigated in the frequency domain; similar reflection is examined when the PML has finite thickness.

0021-9991/98 $25.00
Copyright © 1998 by Academic Press
All rights of reproduction in any form reserved.

Then, the effectiveness of the acoustic PML for a bounded interface is investigated by comparing PML and exact impedance curves for the dilatational motion of a spherical surface. Finally, performance of the PML in time-domain calculations is examined for normal impingement of a plane wave and for absorption of circular waves at the boundaries of circular and rectangular domains.

2. ACOUSTIC PML

Because of the isomorphism between acoustic and electromagnetic wave propagation [4], the adaptation of Berenger's electromagnetics formulation to acoustics is straightforward. With fluid velocity $\mathbf{u}$ normalized to the speed of sound c, fluid pressure p to ρc^2 (where ρ is the mass density), and time t to l/c (where l is a characteristic length measure), the nondimensional pressure–velocity equations of acoustics are

$$\frac{\partial}{\partial t}\mathbf{u} = -\nabla p, \quad \frac{\partial p}{\partial t} = -(\nabla \cdot \mathbf{u}). \tag{1}$$

Following Berenger [1], we expand pressure as $p = p_x + p_y + p_z$ and introduce the attenuation parameters q_x, q_y, q_z to write the PML pressure–velocity equations in a Cartesian reference frame as

$$\begin{aligned}
\frac{\partial u_x}{\partial t} + q_x u_x &= -\frac{\partial}{\partial x}(p_x + p_y + p_z), \quad \frac{\partial p_x}{\partial t} + q_x p_x = -\frac{\partial u_x}{\partial x}, \\
\frac{\partial u_y}{\partial t} + q_y u_y &= -\frac{\partial}{\partial y}(p_x + p_y + p_z), \quad \frac{\partial p_y}{\partial t} + q_y p_y = -\frac{\partial u_y}{\partial y}, \\
\frac{\partial u_z}{\partial t} + q_z u_z &= -\frac{\partial}{\partial z}(p_x + p_y + p_z), \quad \frac{\partial p_z}{\partial t} + q_z p_z = -\frac{\partial u_z}{\partial z}.
\end{aligned} \tag{2}$$

Note that, while u_x, u_y, and u_z are the physical components of velocity, p_x, p_y, p_z, q_x, q_y, and q_z have no physical meaning. Also, when $q_x = q_y = q_z = 0$, the three equations in the left column of (2) reduce to the first of (1) and the sum of the three equations in the right column reduce to the second of (1). Finally, in contrast to the case of three-dimensional electromagnetic waves, where 12 equations are required to describe the PML [2], only six equations are needed here for 3D acoustic waves; this, of course, is because pressure is a scalar field.

3. FREQUENCY-DOMAIN ANALYSIS OF PLANE-WAVE REFLECTION

It is easily verified that the solutions to (2) for time-harmonic plane waves are of the form

$$\psi = \psi_0 \exp[i\omega(\boldsymbol{\gamma} \cdot \mathbf{r} - t)] \exp[-(\mathbf{q} \cdot \mathbf{r})], \tag{3}$$

where $\mathbf{r} = \mathbf{i}x + \mathbf{j}y + \mathbf{k}z$ is the position vector, $\boldsymbol{\gamma} = \mathbf{i}\gamma_x + \mathbf{j}\gamma_y + \mathbf{k}\gamma_z$ is the vector of direction cosines, and the attenuation vector is $\mathbf{q} = \mathbf{i}q_x\gamma_x + \mathbf{j}q_y\gamma_y + \mathbf{k}q_z\gamma_z$. The corresponding solution from in an acoustic medium is, of course, (3) with $\mathbf{q} = 0$.

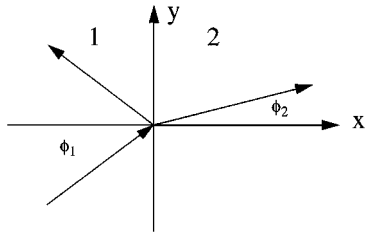

FIG. 1. Plane-wave reflection and transmission.

Let us examine an illuminating two-dimensional problem (Fig. 1). With no z-dependency, Eqs. (2) simplify to

$$\begin{aligned} \frac{\partial u_x}{\partial t} + q_x u_x &= -\frac{\partial}{\partial x}(p_x + p_y), \qquad \frac{\partial p_x}{\partial t} + q_x p_x = -\frac{\partial u_x}{\partial x}, \\ \frac{\partial u_y}{\partial t} + q_y u_y &= -\frac{\partial}{\partial y}(p_x + p_y), \qquad \frac{\partial p_y}{\partial t} + q_y p_y = -\frac{\partial u_y}{\partial y}. \end{aligned} \tag{4}$$

Furthermore, with $\psi_1(x, y) = \psi_{inc}(x, y) + \psi_{refl}(x, y)$ as the generic solution on the left and $\psi_2(x, y) = \psi_{trans}(x, y)$ as that on the right, phase matching of the solutions (3) at $x = 0$ yields (Appendix A)

$$\left(1 + \frac{i}{\omega} q_{y1}\right) \sin\phi_1 = \left(1 + \frac{i}{\omega} q_{y2}\right) \sin\phi_2. \tag{5}$$

In addition, with the pressure and velocity fields in each half-space expressed as (3), continuity of pressure and normal velocity at $x = 0$ produces the reflection coefficient (Appendix A)

$$R_0(\omega) = \frac{\cos\phi_1 - \cos\phi_2}{\cos\phi_1 + \cos\phi_2}. \tag{6}$$

For $q_{y2} = q_{y1}$, (5) yields $\phi_2 = \phi_1$ and then (6) yields $R_0(\omega) = 0$. Thus, if Medium 1 is acoustic and Medium 2 is an acoustic PML, $q_{y2} = 0$ yields perfect phase matching and complete energy absorption at the interface for any values of ϕ_1, ω, and q_{x2}; this is impressive performance.

For a semi-infinite acoustic medium (Medium 1) in contact with a PML of finite thickness (Medium 2), $q_{x1} = q_{y1} = 0$ and Medium 2 extends only over the domain $0 \le x \le \delta$. Then, for $q_{y2} = q_{y1} = 0$, Eqs. (4) become for Medium 2

$$\begin{aligned} \frac{\partial u_x}{\partial t} + q_x u_x &= -\frac{\partial}{\partial x}(p_x + p_y), \quad \frac{\partial p_x}{\partial t} + q_x p_x = -\frac{\partial u_x}{\partial x}, \\ \frac{\partial u_y}{\partial t} &= -\frac{\partial}{\partial y}(p_x + p_y), \quad \frac{\partial p_y}{\partial t} = -\frac{\partial u_y}{\partial y}. \end{aligned} \tag{7}$$

It is readily found that the reflection coefficient at the interface $x = 0$ is given for this problem by (Appendix A)

$$R_0(\omega) = R_\delta \exp\left[-2(q_x - i\omega)\delta \cos\phi_1\right], \tag{8}$$

where R_δ is the reflection coefficient at $x = 1$; $R_\delta = 1$ ($R_\delta = -1$) corresponds to a fixed (free) boundary at $x = \delta$. This relation shows that, for waves with $-\pi/2 < \phi_1 < \pi/2$, $R_0(\omega)$ may be made as small as desired by choosing $q_x\delta$ as large as required. Thus, one can achieve a desired level of attenuation with either a thin, highly attenuating layer or a thick, mildly attenuating layer. Given the goal of minimizing computational cost, the former option is generally to be preferred.

Unfortunately, a jump in attenuation across the medium interface may lead to spurious reflections in discrete models [1]. Hence, it is useful to employ a variable attenuation that increases steadily from zero as one moves away from the interface out through the layer. In this case, the problem of the previous paragraph becomes one of wave propagation in an inhomogeneous medium for which the reflection coefficient may be determined from the solution of a Riccati equation [5]. If the variable attenuation in (7) is taken as $q_x(x) = q_\delta x^n$, the Riccati equation reduces to a linear ordinary differential equation that yields [1]

$$R_0(\omega) = R_\delta \exp\left[-2\left(\frac{q_\delta}{n+1} - i\omega\right)\delta\cos\phi_1\right]. \tag{9}$$

Thus, absorption performance remains high in PML's with variable attenuation if $2q_\delta\delta\cos\phi_1/(n+1)$ is made large.

Results for the special case of normal incidence may be obtained from (8) and (9) by merely taking $\phi_1 = 0$. For this situation, it is useful to examine the specific acoustic impedance $z_0(\omega) = p(0, y, \omega)/u_x(0, y, \omega)$ of Medium 2. In all three cases above, $z_0(\omega)$ is given by

$$z_0(\omega) = \frac{1 + R_0(\omega)}{1 - R_0(\omega)}. \tag{10}$$

Thus, for $|R_0(\omega)| \ll 1$, $z_0(\omega) \approx 1$, which means that the dimensional specific acoustic impedance is simply ρc.

4. FREQUENCY-DOMAIN ANALYSIS OF SPHERICAL-WAVE REFLECTION

The preceding analyses for an unbounded plane interface are not representative of actual computational configurations. Perhaps the simplest representation of a bounded-interface problem pertains to the radially symmetric radiation of acoustic waves by a spherical surface undergoing dilatational motion (Fig. 2). Here, the domain inside the surface at $r = 1$ represents the radiator, and the acoustic and perfectly matched layers represent the unbounded acoustic fluid surrounding the radiator. The fidelity with which the two layers represent the unbounded fluid is readily assessed by comparing approximate and exact specific-acoustic-impedance curves [6] looking out from the spherical surface $r = 1$.

For the PML of Fig. 2, the radially symmetric pressure–velocity equations (which pertain to angle-invariant fields) are

$$\frac{\partial u_r}{\partial t} + q u_r = -\frac{\partial p}{\partial r}, \quad \frac{\partial p}{\partial t} + q p = -\frac{1}{r^2}\frac{\partial}{\partial r}(r^2 u_r). \tag{11}$$

For simplicity, we take q as constant; if $q = 0$, (11) pertains to an acoustic medium, as it must. A straightforward wave-propagation analysis yields for the reflection coefficient at

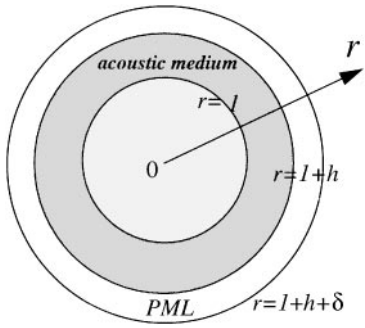

FIG. 2. Acoustic and PML layers on a spherical surface.

$r = 1$ (Appendix A),

$$R_1(\omega) = -\frac{\alpha \cdot 2(q - i\omega)(1 + h)\omega - iq(1 - \alpha)}{2(q - i\omega)(1 + h)\omega - iq(1 - \alpha)} \exp(i2\omega h), \tag{12}$$

where, for a pressure-release surface at $r = 1 + h + \delta$,

$$\alpha = \exp[-2\delta(q - i\omega)], \tag{13}$$

and for a rigid surface at $r = 1 + h + \delta$,

$$\alpha = \frac{(1 + h + \delta)(q - i\omega) + 1}{(1 + h + \delta)(q - i\omega) - 1} \exp[-2\delta(q - i\omega)]. \tag{14}$$

For small reflection from the outer PML boundary ($\alpha \ll 1$), $(q\delta)^2 \gg 1$; then (12) reduces to

$$R_1(\omega) = -[1 + 2\omega(1 + h)(i + \omega/q)]^{-1} \exp(i2\omega h), \tag{15}$$

which is small only for $2\omega(1 + h) \gg 1$ and/or $2\omega^2(1 + h)/q \gg 1$. For frequencies above a specified lower bound, the former is accomplished with a sufficiently large acoustic layer thickness and the latter is accomplished with a very large PML thickness and/or a small attenuation coefficient. As $\omega \to 0$, however, $|R_1(\omega)| \to 1$ and the PML fails.

Greater insight is gained by examining the specific acoustic impedance looking out from the surface of the radiator, i.e., at $r = 1$. It is readily shown that this impedance is given by

$$z_1(\omega) \equiv \eta(\omega) - i\omega\mu(\omega) = \left[\frac{1 - R_1(\omega)}{1 + R_1(\omega)} + \frac{i}{\omega}\right]^{-1}, \tag{16}$$

where $\eta(\omega) = \mathrm{Re}\{z_1(\omega)\}$ is the specific acoustic resistance and $\mu(\omega) = -\omega^{-1}\mathrm{Im}\{z_1(\omega)\}$ is the specific acoustic inertia. For the infinite acoustic medium, these quantities are given by $\eta(\omega) = \omega^2/(1 + \omega^2)$ and $\mu(\omega) = 1/(1 + \omega^2)$ [6] so that (16) yields, as expected, $R_1(\omega) = 0$. We observe that $\eta(\omega)$ approaches zero as $\omega \to 0$ and unity as $\omega \to \infty$ and that $\mu(\omega)$ approaches zero as $\omega \to \infty$ and unity as $\omega \to 0$.

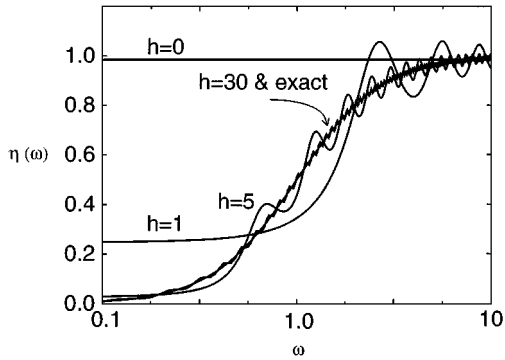

FIG. 3. Specific acoustic resistance curves for the dilatational motion of a spherical surface ($q\delta = 6$).

Specific acoustic resistance and inertia curves produced by (16) and (12) are compared with their exact counterparts in Figs. 3 and 4 for $q\delta = 6$ and $h = 0, 1, 5, 30$. We see that agreement is poor for $h = 0$ and 1, marginal for $h = 5$, and satisfactory for $h = 30$. The curves for $h = 30$ oscillate with small amplitude about the corresponding exact curves, which are smooth. These results suggest that, although the PML is an excellent absorbing boundary for plane-wave reflection at a plane boundary, it might be a poor impedance boundary for more general geometries. A similar analysis has been carried out for radially symmetric circular-wave reflection from a circular interface, with similar results. Hence, in both cases, the PML requires the use of a thick acoustic layer to produce accurate impedance curves for an unbounded acoustic domain.

5. TIME-DOMAIN ANALYSIS OF NORMAL PLANE-WAVE REFLECTION

Let us now consider normal incidence of a transient plane wave on an infinite plane surface at $x = 0$ that separates a semi-infinite acoustic medium and a PML of thickness δ with a constant attenuation parameter q. By direct substitution in the first of (4) with $q_x = 0$ in the acoustic medium and $q_x = q$ in the PML, it is readily shown that the pressure

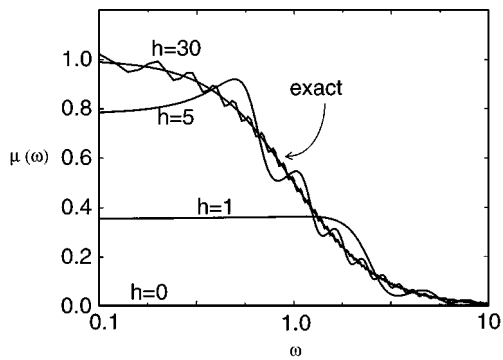

FIG. 4. Specific acoustic inertia curves for the dilatational motion of a spherical surface ($q\delta = 6$).

and velocity fields have the forms

$$\begin{aligned} p_a(x,t) &= f(x-t) + g(x+t), && x \le 0, \\ u_a(x,t) &= f(x-t) - g(x+t), && x \le 0, \\ p_l(x,t) &= e^{-qx}F(x-t) + e^{qx}G(x+t), && x \ge 0, \\ u_l(x,t) &= e^{-qx}F(x-t) - e^{qx}G(x+t), && x \ge 0. \end{aligned} \tag{17}$$

Enforcement of pressure and velocity continuity at $x = 0$ and specification of a rigid or free boundary at $x = \delta$ yield

$$F(\zeta) = f(\zeta), \quad g(\zeta) = G(\zeta), \quad G(\zeta) = \pm e^{-2q\delta} f(2\delta - \zeta), \tag{18}$$

where the plus (minus) pertains to a rigid (free) boundary. Thus, the pressure and velocity fields for this problem are given by

$$\begin{aligned} p_a(x,t) &= f(x-t) \pm e^{-2q\delta} f(2\delta - x - t), && x \le 0, \\ u_a(x,t) &= f(x-t) \mp e^{-2q\delta} f(2\delta - x - t), && x \le 0, \\ p_l(x,t) &= e^{-qx} f(x-t) \pm e^{-q(2\delta - x)} f(2\delta - x - t), && x \ge 0, \\ u_l(x,t) &= e^{-qx} f(x-t) \mp e^{-q(2\delta - x)} f(2\delta - x - t), && x \ge 0. \end{aligned} \tag{19}$$

These results are expected from the frequency-domain analysis of Section 3.

Equations (19) show that PML performance in the continuous system considered depends upon the value of the product $q\delta$, irrespective of the individual values of q and δ. To demonstrate that is not true for the corresponding discretized system, we consider finite-difference calculations for a variable attenuation $q = q(x) = q_\delta (x/\delta)^2$ and a windowed-sine pressure loading at $x = -1$ given by $p(t) = d(t) \sin 2\pi f t$, where $d(t) = 1$ for $0 < t < 1$ and $d(t) = 0$ otherwise; the frequency parameter f assumes the values 1, 5, and 10. A staggered differencing scheme is used that constitutes a reduced version of the scheme described in Appendix B. Computed velocity histories at $x = -1$ are presented in Fig. 5 for $q_\delta = 50$ and $\delta = 0.1$. The figure shows that significant reflection occurs for all three carrier frequencies; note that the reflection for $f = 10$ is actually larger than that for $f = 5$. If q_δ is reduced to 5 and δ increased to 1, thereby maintaining $q_\delta \delta = 5$, the same calculation exhibits visually complete absorption. We used $\Delta x = 0.01$ and $\Delta t = 0.005$ in the computations for Fig. 5 to ensure numerical stability and good resolution.

6. ABSORPTION OF A SOURCE-GENERATED TRANSIENT WAVE IN TWO DIMENSIONS

In order to verify our implementation of the PML technique, we performed an acoustic version of Berenger's 1994 calculation [1]. Two separate computations were carried out using the finite-difference scheme outlined in Appendix B. One pertained to a 100×50-cell rectangular domain enclosed by a PML on all sides, and the other, a reference solution, pertained to a 380×380-cell square domain. A pulse excitation was applied at the geometrical center of both domains. After nondimensionlization of Berenger's electromagnetic-wave formulation on the basis of the speed of light (3×10^8 m/s) and the horizontal length of the

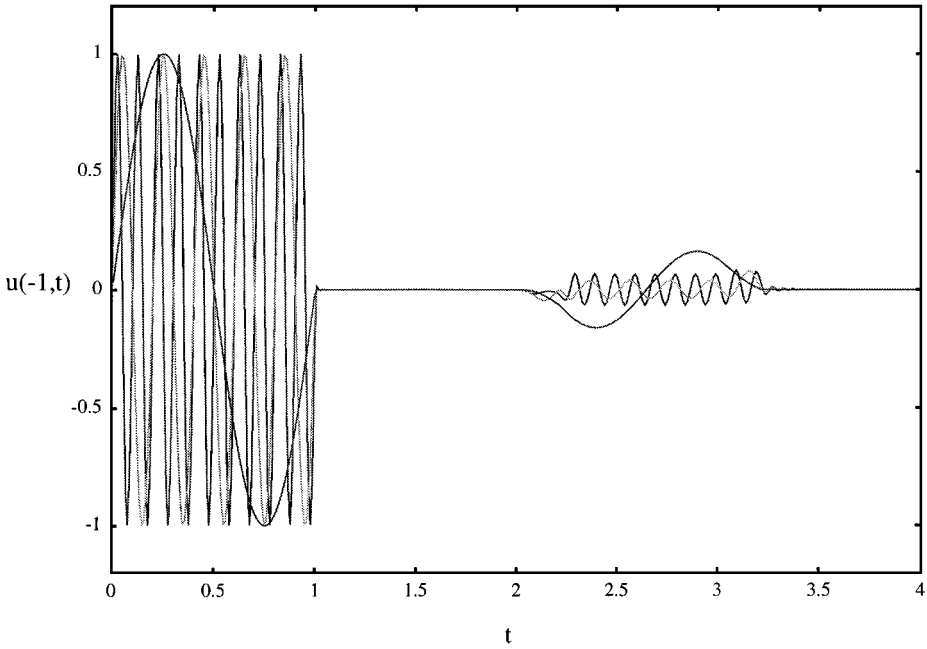

FIG. 5. Velocity histories at the point of application of a windowed-sine pressure loading for three different frequencies: $f = 1, 5, 10$ (plane waves; $q_\delta = 50$ and $\delta = 0.1$).

100-cell side (1.5 m), the pulse in dimensionless form is given by

$$\begin{aligned} p(n_x, n_y) &= (10 - 15\cos 10\pi t + 6\cos 20\pi t - \cos 30\pi t)/320 \quad \text{for } t < 0.2, \\ p(n_x, n_y) &= 0 \qquad\qquad\qquad\qquad\qquad\qquad\qquad\qquad\quad \text{for } t > 0.2. \end{aligned} \tag{20}$$

A plot of this pulse displays a characteristic period of $T_c \approx 0.2$ and thus a characteristic frequency of $f_c \approx 5$. The loading points (n_x, n_y) are (50, 25) and (190, 190) for the two computations. The dimensionless spatial and temporal increments are 0.01 and 0.005, which correspond to Berenger's spatial and temporal increments of 1.5 cm and 25 ps, respectively. Free-boundary solutions, corresponding to acoustic pressure-release boundaries, were obtained.

Two curves are presented in Fig. 6 for the relative error along the lower interface of the acoustic and PML domains at $t = 2.5$; this error is defined as

$$R(i) = [p(i, 1) - p_r(i, 1)]/p_r(50, 1)_{\max}, \tag{21}$$

where $p(i, 1)$ is the pressure snapshot obtained with the 100×50-cell domain enclosed by the PML and $p_r(i, 1)$ is the corresponding reference snapshot obtained with the 380×380-cell domain. The first curve (a) is obtained with a PML of linear spatial variation, $q(z) = q_\delta(z/\delta)$, where z is a local thickness coordinate and δ is the thickness of the PML; the other curve (b) is obtained with a PML of parabolic spatial variation $q(z) = q_\delta(z/\delta)^2$, which is the same PML used in our earlier calculations. In both cases, 10 PML cells corresponding to $q_\delta = 50$ and $\delta = 0.1$ are employed to enclose the 100×50-cell computational domain. Note that the linear PML performs slightly better than the parabolic PML for this pulse

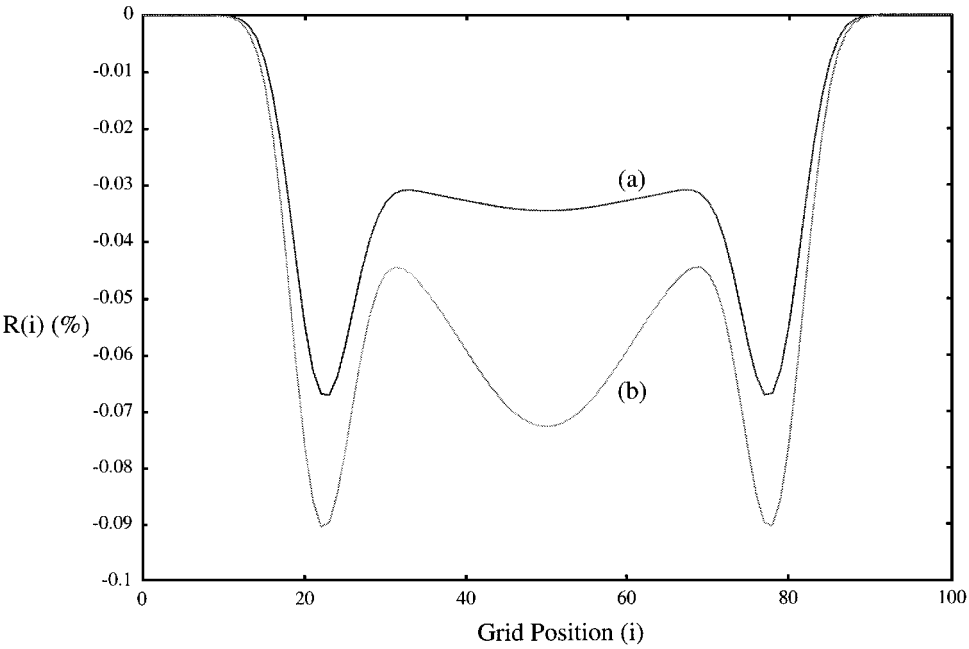

FIG. 6. Absorption of a pulse excitation by the PML technique shown as percentage relative error $R(i)$ ($t = 2.5$, $q_\delta = 50$, $\delta = 0.1$ and $q(z) = q_\delta(z/\delta)^n$) (a) $n = 1$; (b) $n = 2$.

excitation. However, both solutions demonstrate that the PML is very effective in this case. The solution obtained here falls within the accuracy range achieved by Berenger with both linear and parabolic PMLs (Figs. 9–11 in [1]).

7. TIME-DOMAIN ANALYSIS OF CIRCULAR-WAVE REFLECTION

To examine further PML performance in computational acoustics, time-domain finite-difference computations for a two-dimensional, radially symmetric geometry are performed. Here, we discretize the following governing equations in the PML between $r = 1 + h$ and $r = 1 + h + \delta$ for the two-dimensional configuration of Fig. 2:

$$\frac{\partial u}{\partial t} + q(r)u = -\frac{\partial p}{\partial r}, \quad \frac{\partial p}{\partial t} + q(r)p = -\frac{1}{r}\frac{\partial}{\partial r}(ru), \tag{22}$$

where

$$q(r) = q_\delta[r - (1 + h)]^2/\delta^2. \tag{23}$$

Corresponding governing equations for the acoustic medium between $r = 1$ and $r = 1+h$ are obtained by taking $q(r) = 0$. A radially symmetric version of the finite-difference scheme described in Appendix B is used.

In the computations that produced Figs. 7, 8, and 9, $\Delta r = 0.01$, $\Delta t = 0.005$, and $q_m = 50$. Again, a windowed-sine pressure loading is the excitation. Significant reflections

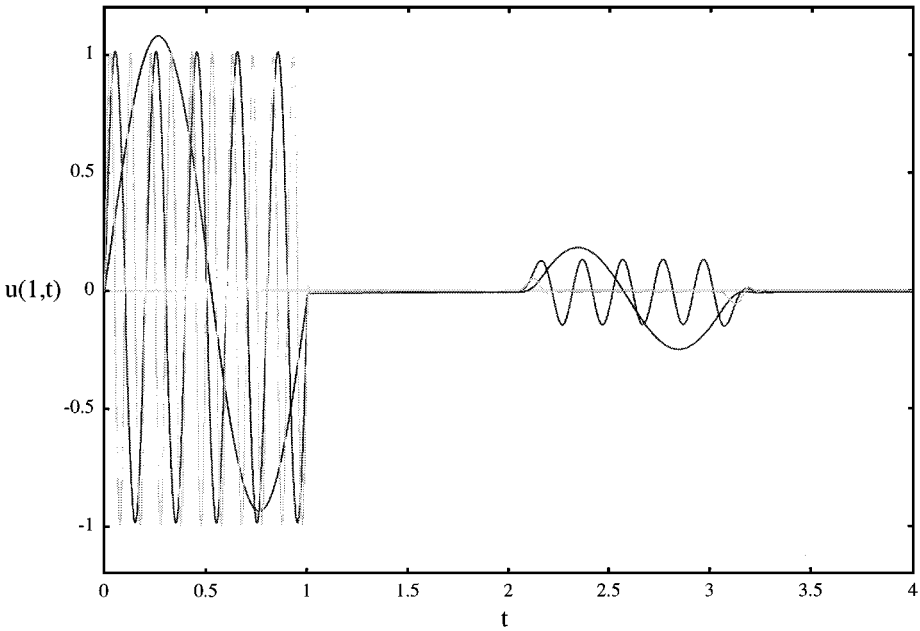

FIG. 7. Velocity histories at $r = 1$ for a windowed-sine radially symmetric pressure loading for three different frequencies: $f = 1, 5, 10$ (circular waves; $q_\delta = 50$, $h = 1$, and $\delta = 0.1$).

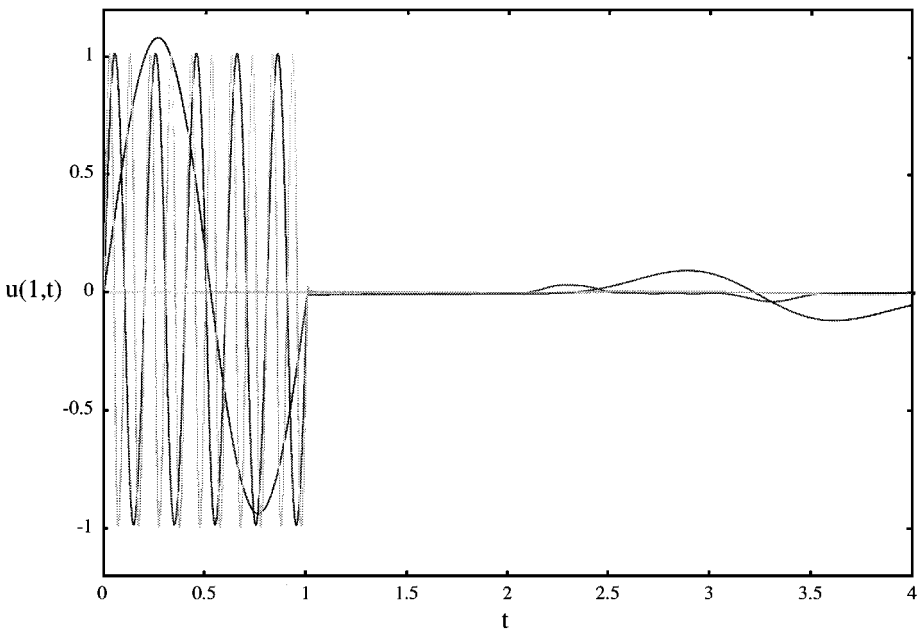

FIG. 8. Velocity histories at $r = 1$ for a windowed-sine radially symmetric pressure loading for three different frequencies: $f = 1, 5, 10$ (circular waves; $q_\delta = 50$, $h = 1$, and $\delta = 2$).

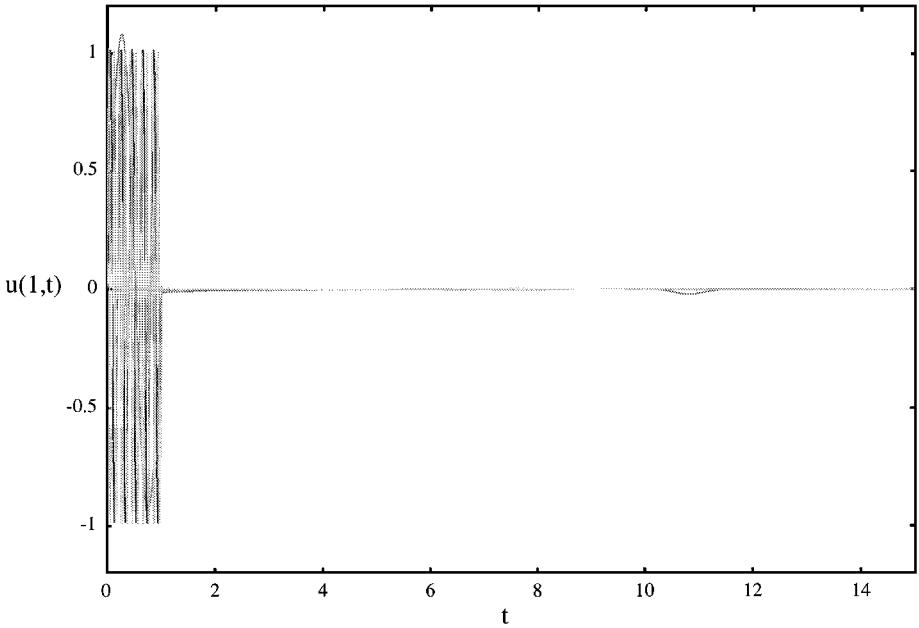

FIG. 9. Velocity histories at $r = 1$ for a windowed-sine radially symmetric pressure loading for three different frequencies: $f = 1, 5, 10$ (circular waves; $q_\delta = 50$, $h = 5$, and $\delta = 0.1$).

are observed from the acoustic/PML interface in Figs. 7 and 8. It is interesting to note that merely increasing the thickness of the PML does not achieve high absorption of a low-frequency incident wave ($f = 1$) as it does for a plane incident wave. Thus, a PML surrounding a relatively thin acoustic layer ($h \sim 1$) cannot accurately represent the infinite domain at low frequencies. Much improved velocity histories are obtained with $h = 5$, as shown in Fig. 9, which agrees with the frequency-based behavior seen in Figs. 3 and 4.

Most time-domain calculations use a rectangular domain rather than a circular one. Thus, we now consider circular waves that impinge on a square boundary (Fig. 10). Because of symmetry, only a quarter of the domain need be considered. A two-dimensional staggered scheme [7, 1] is used, the details of which are given in Appendix B. For windowed-sine pressure loadings generated at $r = 1$, velocity histories on $r = 1$ at three different angular locations, $\theta = 0^\circ, 22.5^\circ,$ and 45°, are shown in Figs. 11, 12, and 13 for $f = 1, 5,$ and 10, respectively. In these calculations, we used $q(z) = 50(z/\delta)^2$ and $h = 4$, where the PML thickness δ is 0.1 and z is a local thickness coordinate. Note that $h = 4$ approximately corresponds to the same area of acoustic medium characterizing the case of circular symmetry with $h = 5$. Before reflection takes place, differences in velocity histories for the three different angles are seen to be very small, which validates the use of a stepped boundary to represent the quarter circle. From the results, it is seen that the amplitude of the reflected signal decreases with increasing carrier frequency. However, the amplitude of the reflected signal for a given carrier frequency is larger than that of its counterpart in the case of radial symmetry.

Now the results shown in Figs. 7–9 and 11–13 are not directly comparable to those appearing in Fig. 6, inasmuch as the former pertain to the normal-velocity field on a radiator's

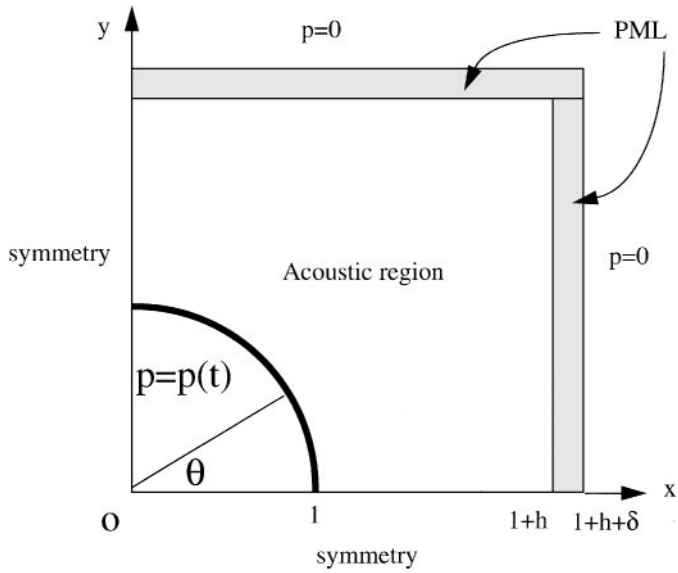

FIG. 10. Computational domain for two-dimensional finite-difference computations with a PML.

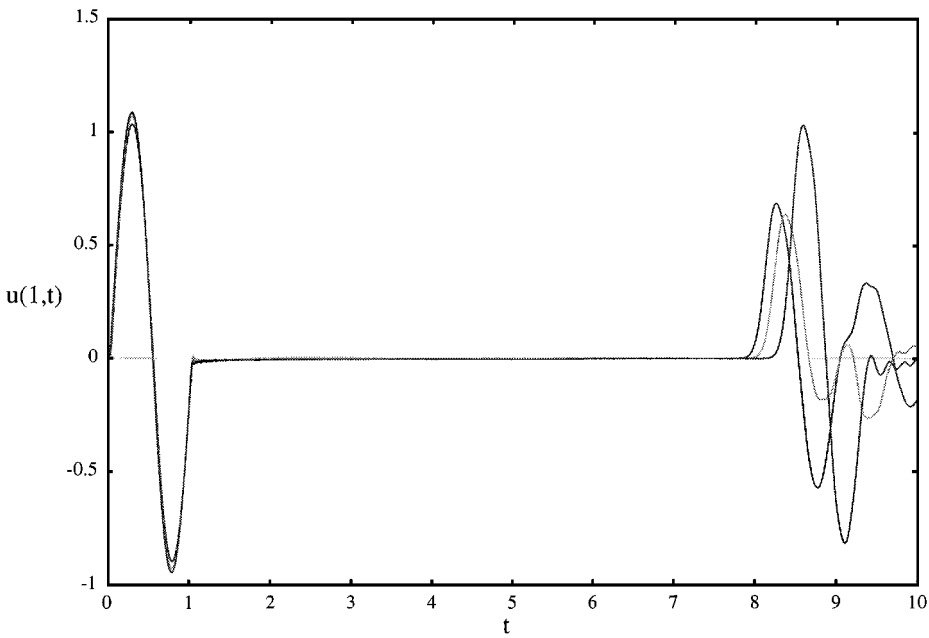

FIG. 11. Velocity histories on $r = 1$ at $\theta = 0^\circ$, 22.5°, and 45° for a windowed-sine pressure loading (square boundary; $h = 4$, $q_\delta = 50$, $\delta = 0.5$, and $f = 1$).

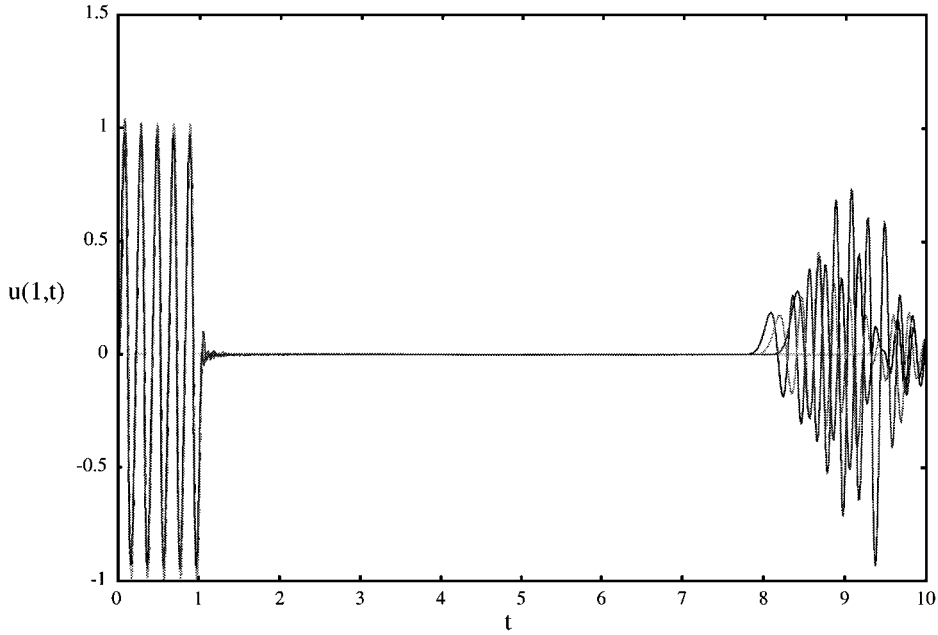

FIG. 12. Velocity histories on $r = 1$ at $\theta = 0^\circ$, 22.5°, and 45° for a windowed-sine pressure loading (square boundary; $h = 4$, $q_\delta = 50$, $\delta = 0.5$, and $f = 5$).

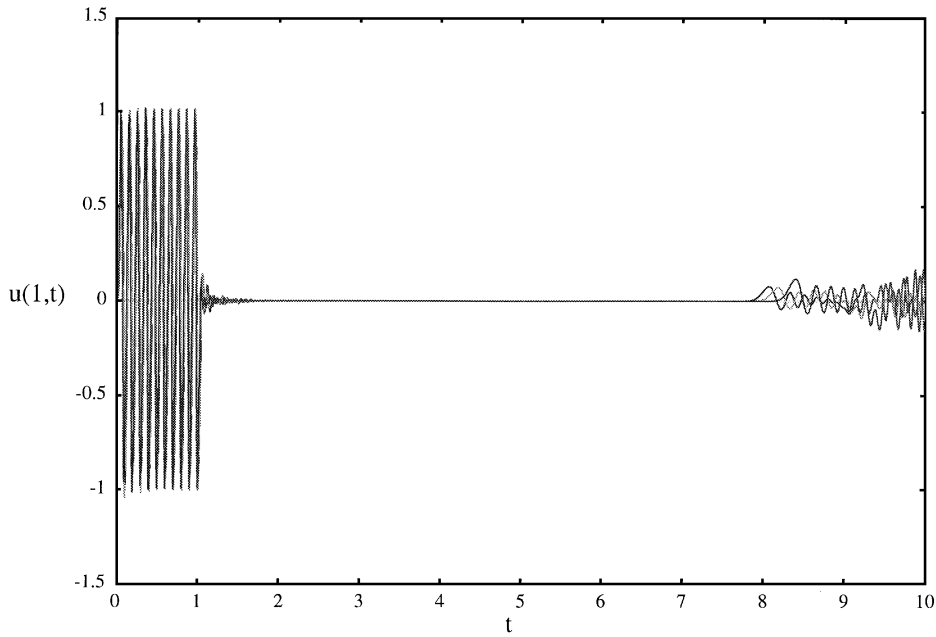

FIG. 13. Velocity histories on $r = 1$ at $\theta = 0^\circ$, 22.5°, and 45° for a windowed-sine pressure loading (square boundary; $h = 4$, $q_\delta = 50$, $\delta = 0.5$, and $f = 10$).

surface and the latter pertain to the pressure field at an acoustic-PML interface. However, the results in Fig. 6 indicate high absorption of the radiated wave, whereas those in Figs. 7–9 and 11–13 indicate low absorption. The discrepancy is due to the vast difference between the ratios of the acoustic-layer's characteristic thickness to the radiator's characteristic radius. In the problem associated with Fig. 6, the radiator's characteristic radius is roughly one-half of a cell width and the acoustic-layer's characteristic thickness is 25 to 50 cell widths, so that the thickness to radius ratio lies between 50 and 100. In the problem associated with Figs. 7–9 and 11–13, the corresponding ratios range from 1 to 6. Thus, as demonstrated in Figs. 3 and 4, increasing the thickness of the acoustic layer until it is much larger than the characteristic radius of the radiator greatly improves PML performance.

8. CONCLUSION

The performance of the perfectly matched layer (PML), first formulated by Berenger for the time-domain, finite-difference solution of Maxwell's equations, has been evaluated for computational acoustics. It is shown that, while the PML constitutes an excellent absorbing boundary for plane waves incident upon a planar interface, its performance in nonplanar geometries is not always satisfactory.

A PML is surely effective in nonplanar geometries when $(q_\delta \delta)^2 \gg 1$ (where $\delta \sim 1$) and $h \gg 1$. It can also be effective with smaller h in the case of short acoustic wavelengths, i.e., for $f \gg 1$ (Figs. 3, 4, 8, and 13); in this circumstance, $\delta \ll 1$ sometimes works satisfactorily (Fig. 7), although a larger δ is better (Fig. 8).

The PML *cannot work well in nonplanar geometries for* $h < 1$ *and* $f < 1$ *because the radiated/scattered near field at intermediate and low frequencies is not purely radiative*. In Figs. 3 and 4, the specific acoustic impedance presented by the PML for $h = 0$ is purely resistive, whereas the impedance for the infinite acoustic domain is both resistive and inertial over the range $0.1 \leq \omega \leq 10$; for $\omega \leq 0.1$ the impedance is almost purely inertial. The combination of a PML-encased acoustic layer with $h = 1$ produces a more representative impedance, but an acoustic layer with $h > 5$ is required to achieve an accurate impedance over the range $0.1 \leq \omega \leq 10$.

The requirement of a thick acoustic layer ($h \gg 1$) is not a computational burden if one is interested in the acoustic field over a large region surrounding the radiator/scatterer. However, this is often not the case. When one is interested only in the response of the radiator/scatterer, one would like to use $h = 0$ for maximum computational efficiency. Even if one is interested in far-field radiation/scattering, it is often more computationally efficient first to determine the radiated/scattered acoustic field on the surface of the radiator/scatterer and then to calculate far-field results from the solution at that surface.

APPENDIX A: REFLECTION COEFFICIENTS

To derive (5), we write from (3)

$$\begin{aligned}
\psi_{inc}(x, y, t) &= \psi_{io} \exp[i\omega(\cos\phi_1 x + \sin\phi_1 y - t) - q_{x1}\cos\phi_1 x - q_{y1}\sin\phi_1 y], \\
\psi_{refl}(x, y, t) &= \psi_{ro} \exp[i\omega(-\cos\phi_1 x + \sin\phi_1 y - t) + q_{x1}\cos\phi_1 x - q_{y1}\sin\phi_1 y], \\
\psi_{trans}(x, y, t) &= \psi_{to} \exp[i\omega(\cos\phi_2 x + \sin\phi_2 y - t) - q_{x2}\cos\phi_2 x - q_{y2}\sin\phi_2 y],
\end{aligned} \tag{A1}$$

so that

$$\psi_{inc}(0,y,t)=\psi_{io}\exp\Phi_1,\quad \psi_{refl}(0,y,t)=\psi_{ro}\exp\Phi_1,$$
$$\psi_{trans}(0,y,t)=\psi_{to}\exp\Phi_2, \tag{A2}$$

where $\Phi_k=i\omega(\sin\phi_k y-t)-q_{yk}\sin\phi_k y$. Setting $\Phi_1=\Phi_2$, we obtain (5).

To derive (6), we write from (A2) with $\Phi_2=\Phi_1$, $p_{inc}(0,y,t)=p_{io}\exp(\Phi_1)$, $p_{refl}(0,y,t)=p_{ro}\exp(\Phi_1)$, and $p_{trans}(0,y,t)=p_{to}\exp(\Phi_1)$. Thus, $p_{inc}(0,y,t)+p_{refl}(0,y,t)=p_{trans}(0,y,t)$ yields $p_{io}+p_{ro}=p_{to}$. Also, we find from (A1)

$$\begin{aligned}
&\frac{\partial}{\partial x}[p_{x1}(x,y,t)+p_{y1}(x,y,t)]\\
&\quad=\frac{\partial}{\partial x}[p_1(x,y,t)]=\frac{\partial}{\partial x}[p_{inc}(x,y,t)+p_{refl}(x,y,t)]\\
&\quad=(i\omega-q_{x1})\cos\phi_1 p_{io}\exp[i\omega(\cos\phi_1 x+\sin\phi_1 y-t)-q_{x1}\cos\phi_1 x-q_{y1}\cos\phi_1 y]\\
&\qquad+(-i\omega+q_{x1})\cos\phi_1 p_{ro}\exp[i\omega(-\cos\phi_1 x+\sin\phi_1 y-t)\\
&\qquad\qquad+q_{x1}\cos\phi_1 x-q_{y1}\cos\phi_1 y],
\end{aligned}\tag{A3}$$

$$\begin{aligned}
&\frac{\partial}{\partial x}[p_{x2}(x,y,t)+p_{y2}(x,y,t)]\\
&\quad=\frac{\partial}{\partial x}[p_2(x,y,t)]=\frac{\partial}{\partial x}[p_{trans}(x,y,t)]\\
&\quad=(i\omega-q_{x2})\cos\phi_2 p_{to}\exp[i\omega(\cos\phi_2 x+\sin\phi_2 y-t)-q_{x2}\cos\phi_2 x-q_{y2}\cos\phi_2 y],
\end{aligned}$$

so that these, (5), and the first of (4) give

$$u_{x1}(0,y,t)=(p_{io}-p_{ro})\cos\phi_1\exp(\Phi_1),\quad u_{x2}(0,y,t)=p_{to}\cos\phi_2\exp(\Phi_1). \tag{A4}$$

Thus, $u_{x1}(0,y,t)=u_{x2}(0,y,t)$ yields $(p_{io}-p_{ro})\cos\phi_1=p_{to}\cos\phi_2$. This result, along with $p_{io}+p_{ro}=p_{to}$ and $R\equiv p_{ro}/p_{io}$, produces (6).

For the problem of an acoustic medium (Medium 1) occupying the domain $-\infty\le x\le 0$ that is in contact with an acoustic PML (Medium 2) occupying the domain $0\le x\le\delta$, we write for $-\infty\le x\le 0$

$$\begin{aligned}
p_{inc}(x,y,t)&=p_{io}\exp[i\omega(\cos\phi_1 x+\sin\phi_1 y-t)],\\
p_{refl}(x,y,t)&=p_{ro1}\exp[i\omega(-\cos\phi_1 x+\sin\phi_1 y-t)],
\end{aligned}\tag{A5}$$

and for $0\le x\le\delta$ [with $q_{y2}=q_{y1}=0$, which yields $\phi_2=\phi_1$ from (5)]

$$\begin{aligned}
p_{trans}(x,y,t)&=p_{to}\exp[i\omega(\cos\phi_1 x+\sin\phi_1 y-t)-q_x\cos\phi_1 x],\\
p_{refl2}(x,y,t)&=p_{ro2}\exp[i\omega(-\cos\phi_1 x+\sin\phi_1 y-t)+q_x\cos\phi_1 x].
\end{aligned}\tag{A6}$$

These equations plus the first of (7) then yield

$$\begin{aligned} p_{inc}(0,y,t) &= p_{io}\exp(\Phi),\ p_{refl1}(0,y,t) = p_{ro1}\exp(\Phi),\\ p_{trans}(0,y,t) &= p_{to}\exp(\Phi),\ p_{refl2}(0,y,t) = p_{ro2}\exp(\Phi),\\ u_{x1}(0,y,t) &= (p_{io}-p_{ro1})\cos\phi_1\exp(\Phi),\\ u_{x2}(0,y,t) &= (p_{to}-p_{ro2})\cos\phi_1\exp(\Phi), \end{aligned} \tag{A7}$$

where $\Phi = i\omega(\sin\phi_1 y - t)$.

Continuity of pressure and normal velocity at $x=0$ then produces from (A7) $p_{io}+p_{ro1} = p_{to}+p_{ro2}$ and $p_{io}-p_{ro1} = p_{to}-p_{ro2}$, which may be added and subtracted to obtain $p_{to} = p_{io}$ and $p_{ro2} = p_{ro1}$. The boundary condition at $x=\delta$ may be written $p_{refl2}(\delta,y,t) = R_\delta p_{trans}(\delta,y,t)$, where $R_\delta = 1$ for a fixed boundary and $R_\delta = -1$ for a free boundary. But, from (A6), $p_{trans}(\delta,y,t) = p_{to}\exp[(i\omega - q_x)\,\delta\cos\phi_1 + \Phi]$ and $p_{refl2}(\delta,y,t) = p_{ro2}\exp[(-i\omega+q_x)\,\delta\cos\phi_1+\Phi]$; thus, $p_{ro2} = R_\delta\exp[2(i\omega-q_x)\,\delta\cos\phi_1]p_{to}$. Finally, the introduction of $p_{ro2}=p_{ro1}$ and $p_{to}=p_{io}$ into this result yields (8) for the reflection coefficient $R_0(\omega) = p_{ro1}/p_{io}$.

Regarding (12), we proceed as follows. By direct substitution in (11) (with $q=0$ for the acoustic medium), it is readily shown that the time-harmonic pressure and velocity fields have the form

$$\begin{aligned} p_a(r,t) &= Ar^{-1}e^{i\omega(r-t)} + Br^{-1}e^{-i\omega(r+t)}, && 1\le r\le 1+h,\\ u_a(r,t) &= (1+i/\omega r)Ar^{-1}e^{i\omega(r-t)}\\ &\quad -(1-i/\omega r)Br^{-1}e^{-i\omega(r+t)}, && 1\le r\le 1+h,\\ p_l(r,t) &= Cr^{-1}e^{-qr}e^{i\omega(r-t)} + Dr^{-1}e^{qr}e^{-i\omega(r+t)}, && 1+h\le r\le 1+h+\delta,\\ u_l(r,t) &= [1+1/(q-i\omega)r]Cr^{-1}e^{-qr}e^{i\omega(r-t)}\\ &\quad -[1-1/(q-i\omega)r]Dr^{-1}e^{qr}e^{-i\omega(r+t)}, && 1+h\le r\le 1+h+\delta. \end{aligned} \tag{A8}$$

Enforcement of pressure and velocity continuity at $r = 1+h$ yields

$$\begin{aligned} &Ae^{i\omega(1+h)} + Be^{-i\omega(1+h)} = Ce^{-q(1+h)}e^{i\omega(1+h)} + De^{q(1+h)}e^{-i\omega(1+h)},\\ &[1+i/\omega(1+h)]Ae^{i\omega(1+h)} - [1-i/\omega(1+h)]Be^{-i\omega(1+h)}\\ &\quad = [1+1/(q-i\omega)(1+h)]Ce^{-q(1+h)}e^{i\omega(1+h)}\\ &\qquad -[1-1/(q-i\omega)(1+h)]De^{q(1+h)}e^{-i\omega(1+h)} \end{aligned} \tag{A9}$$

and the boundary condition at $r = 1+h+\delta$ gives $D = \alpha C$, where α is given by (13) for a pressure-release boundary and by (14) for a rigid boundary. Simultaneous solution of this last equation and (A9) yields (12) for the reflection coefficient $R_1(\omega) = B/A$.

APPENDIX B: STAGGERED FINITE-DIFFERENCING SCHEME

Consistent with Berenger's approach, a staggered finite difference scheme (Yee's algorithm) is used here [7]. A typical cell is shown in Fig. B1. Note that pressure is computed at

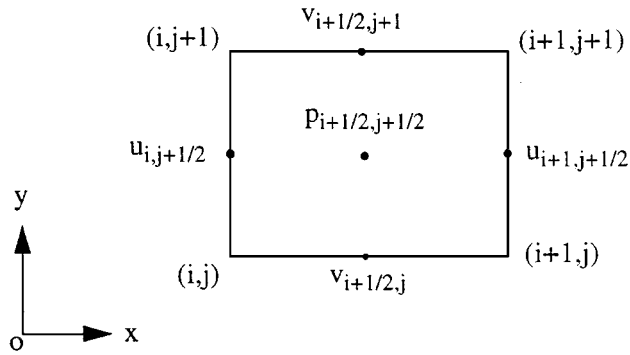

FIG. B1. Computation cell.

the center of the computational cell, while velocities are computed at the midpoints along the edge of the cell. For $\Delta x = \Delta y$, we have for the acoustic domain

$$
\begin{aligned}
p^{n+1/2}_{i+1/2,\,j+1/2} &= p^{n-1/2}_{i+1/2,\,j+1/2} - \frac{\Delta t}{\Delta x}\left(u^{n}_{i+1,\,j+1/2} - u_{i,\,j+1/2} + v^{n}_{i+1/2,\,j+1} - v^{n}_{i+1/2,\,j}\right)\\
u^{n+1}_{i,\,j+1/2} &= u^{n-1}_{i,\,j+1/2} - \frac{\Delta t}{\Delta x}\left[p^{n+1/2}_{i+1/2,\,j+1/2} - p^{n+1/2}_{i-1/2,\,j+1/2}\right]\\
v^{n+1}_{i+1/2,\,j} &= v^{n-1}_{i+1/2,\,j} - \frac{\Delta t}{\Delta x}\left[p^{n+1/2}_{i+1/2,\,j+1/2} - p^{n+1/2}_{i+1/2,\,j-1/2}\right].
\end{aligned}
\tag{B1}
$$

In the PML, $p = p_x + p_y$, we split the equations accordingly. Therefore,

$$
\begin{aligned}
p^{n+1/2}_{xi+1/2,\,j+1/2} &= p^{n-1/2}_{xi+1/2,\,j+1/2}e^{-q_{xi+1/2}\Delta t} - \left(\frac{1-e^{-q_{xi+1/2}\Delta t}}{q_{xi+1/2}\Delta x}\right)\left[u^{n}_{i+1,\,j+1/2} - u^{n}_{i,\,j+1/2}\right]\\
p^{n+1/2}_{yi+1/2,\,j+1/2} &= p^{n-1/2}_{yi+1/2,\,j+1/2}e^{-q_{yi+1/2}\Delta t} - \left(\frac{1-e^{-q_{yi+1/2}\Delta t}}{q_{yi+1/2}\Delta x}\right)\left[v^{n}_{i+1/2,\,j+1} - v^{n}_{i+1/2,\,j}\right]\\
u^{n+1}_{i,\,j+1/2} &= u^{n}_{i,\,j+1/2} - \left(\frac{1-e^{-q_{xi+1/2}\Delta t}}{q_{xi+1/2}\Delta x}\right)\\
&\quad\times\left[p^{n+1/2}_{xi+1/2,\,j+1/2} + p^{n+1/2}_{yi+1/2,\,j+1/2} - p^{n+1/2}_{xi-1/2,\,j+1/2} - p^{n+1/2}_{yi-1/2,\,j+1/2}\right].\\
v^{n+1}_{i+1/2,\,j} &= v^{n}_{i+1/2,\,j} - \left(\frac{1-e^{-q_{yi+1/2}\Delta t}}{q_{yj+1/2}\Delta x}\right)\\
&\quad\times\left[p^{n+1/2}_{xi+1/2,\,j+1/2} + p^{n+1/2}_{yi+1/2,\,j+1/2} - p^{n+1/2}_{xi+1/2,\,j-1/2} - p^{n+1/2}_{yi+1/2,\,j-1/2}\right].
\end{aligned}
\tag{B2}
$$

The truncation error of the above finite-difference scheme is $O[(\Delta t)^2, (\Delta x)^2]$. Care needs to be taken when dealing with nodes at the acoustic/PML interface; i.e., (B2) must be modified to allow transition from two pressure components in the PML to one in the acoustic domain [1]. For nodes at the acoustic PML interface denoted by N, the first two of (B2) are still

applicable, but the third and fourth become

$$u_{N,j+1/2}^{n+1} = u_{N,j+1/2}^{n} - \left(\frac{1 - e^{-q_{xN+1/2}\Delta t}}{q_{xN+1/2}\Delta x}\right)\left[p_{xN+1/2,j+1/2}^{n+1/2} + p_{yN+1/2,j+1/2}^{n+1/2} - p_{xN-1/2,j+1/2}^{n+1/2}\right] \tag{B3}$$

$$v_{i+1/2,N}^{n+1} = v_{i+1/2,N}^{n} - \left(\frac{1 - e^{-q_{yN+1/2}\Delta t}}{q_{yN+1/2}\Delta x}\right)\left[p_{xi+1/2,N+1/2}^{n+1/2} + p_{yi+1/2,N+1/2}^{n+1/2} - p_{xi+1/2,N-1/2}^{n+1/2}\right].$$

ACKNOWLEDGMENTS

This work was sponsored by the Defense Special Weapons Agency under Contract DNA001-94-C-0004 with Douglas Bruder acting as the Contracting Officer's Technical Representative. The authors thank their colleague Kendall Hunter for helping with the final preparation of the manuscript.

REFERENCES

1. J.-P. Berenger, A perfectly matched layer for the absorption of electromagnetic waves, *J. Comput. Phys.* **114**, 185 (1994).
2. D. S. Katz, E. T. Thiele, and A. Taflove, Validation and extension to three dimensions of the Berenger PML absorbing boundary condition for FD-TD meshes, *IEEE Microwave Guided Wave Lett.* **4**, 268 (1994).
3. F. Q. Hu, On absorbing boundary conditions for linearized Euler equations by a perfectly matched layer, *J. Comput. Phys.* **129**, 201 (1996).
4. D. H. Towne, *Wave Phenomena* (Dover, New York, 1967).
5. I. Tolstoy and C. S. Clay, *Ocean Acoustics* (Am. Inst. Phys., New York 1967).
6. T. L. Geers, Doubly asymptotic approximations for transient motions of submerged structures, *J. Acoust. Soc. Am.* **64**, 1500 (1978).
7. A. Taflove, Review of the formulation and applications of the finite-difference time-domain method for numerical modeling of electromagnetic wave interactions with arbitrary structures, *Wave Motion* **10**, 547 (1988).